

# Discovery of Potent and Selective 7-Azaindole Isoindolinone-Based PI3K $\gamma$ Inhibitors

Dillon H. Miles, Xuelei Yan, Rhiannon Thomas-Tran, Jeremy Fournier, Ehesan U. Sharif, Samuel L. Drew, Guillaume Mata, Kenneth V. Lawson, Elaine Ginn, Kent Wong, Divyank Soni, Puja Dhanota, Stefan G. Shaqfeh, Cesar Meleza, Ada Chen, Amber T. Pham, Timothy Park, Debbie Swinarski, Jesus Banuelos, Ulrike Schindler, Matthew J. Walters, Nigel P. Walker, Xiaoning Zhao, Stephen W. Young, Jie Chen, Lixia Jin, Manmohan Reddy Leleti, Jay P. Powers, and Jenna L. Jeffrey\*

Cite This: *ACS Med. Chem. Lett.* 2020, 11, 2244–2252

Read Online

ACCESS |

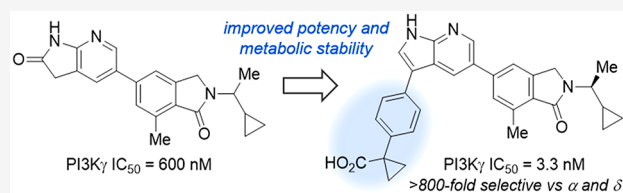
Metrics & More

Article Recommendations

Supporting Information

**ABSTRACT:** The successful application of immunotherapy in the treatment of cancer relies on effective engagement of immune cells in the tumor microenvironment. Phosphoinositide 3-kinase  $\gamma$  (PI3K $\gamma$ ) is highly expressed in tumor-associated macrophages, and its expression levels are associated with tumor immunosuppression and growth. Selective inhibition of PI3K $\gamma$  offers a promising strategy in immunoncology, which has led to the development of numerous potent PI3K $\gamma$  inhibitors with variable selectivity profiles. To facilitate further investigation of the therapeutic potential of PI3K $\gamma$  inhibition, we required a potent and PI3K $\gamma$ -selective tool compound with sufficient metabolic stability for use in future *in vivo* studies. Herein, we describe some of our efforts to realize this goal through the systematic study of SARs within a series of 7-azaindole-based PI3K $\gamma$  inhibitors. The large volume of data generated from this study helped guide our subsequent lead optimization efforts and will inform further development of PI3K $\gamma$ -selective inhibitors for use in immunomodulation.

**KEYWORDS:** PI3K $\gamma$ , inhibitor, selective, azaindole, immunomodulation, cancer



Phosphoinositide 3-kinases (PI3Ks) are a class of enzymes responsible for the regulation of a wide variety of cellular activities such as signaling, survival, metabolism, and transport. A common substrate of these kinases is the glycerophospholipid phosphatidylinositol (PIP): PI3K-mediated phosphorylation of PIP initiates a signaling cascade via downstream proteins (e.g., protein kinase B (PKB), commonly referred to as Akt, and 3-phosphoinositide-dependent protein kinase-1 (PDK1)) and ultimately mediates critical cellular functions, such as motility and proliferation.<sup>1,2</sup> The class I PI3Ks, including PI3K $\alpha$ , PI3K $\beta$ , PI3K $\gamma$ , and PI3K $\delta$ , phosphorylate the C3-hydroxyl group of the inositol ring in phosphatidylinositol 4,5-bisphosphate.<sup>3</sup>

Although PI3Ks are involved in a variety of functions and are expressed throughout the body, PI3K $\gamma$  and PI3K $\delta$  are of particular interest due to their expression in leukocytes as effectors of immune responses.<sup>4–7</sup> In oncology, abnormalities in PI3K expression have been linked to cancer development, corresponding to high levels of PI3K $\gamma$  expression and activity within immunosuppressive myeloid cells.<sup>8–18</sup> Due to the significance of PI3K $\gamma$  and PI3K $\delta$  in immunomodulation, many inhibitors with varying degrees of selectivity have been developed for the treatment of cancers and other pathologies of the immune system.<sup>19,20</sup> Structures of several potent and  $\gamma$ -selective inhibitors have been published, selected examples of

which are shown in Figure 1a.<sup>21–27</sup> Among these, **1** (IPI-549, developed by Infinity Pharmaceuticals) is the only  $\gamma$ -selective inhibitor currently in clinical trials (Ph. 1/2).<sup>28–32</sup> Aryl sulfonamide **2** (developed by Exelixis), an advanced lead compound that resulted from optimization of a high-throughput screening hit, exhibits moderate PI3K isoform selectivity but also inhibits the mammalian target of rapamycin (mTOR) and other off-target kinases.<sup>25</sup> Recently, researchers at AstraZeneca reported a series of aminothiazole-based PI3K $\gamma$  inhibitors such as **3**, which was characterized by X-ray crystallography in complex with mouse PI3K $\delta$  (PDB ID 6FTN).<sup>26,27</sup> The high isoform selectivity of **3** and its analogues was attributed to the ability of the cyclopropylethyl group to displace the DFG motif of PI3K $\gamma$ , which causes a unique  $\gamma$  isoform-specific conformational change.<sup>27</sup>

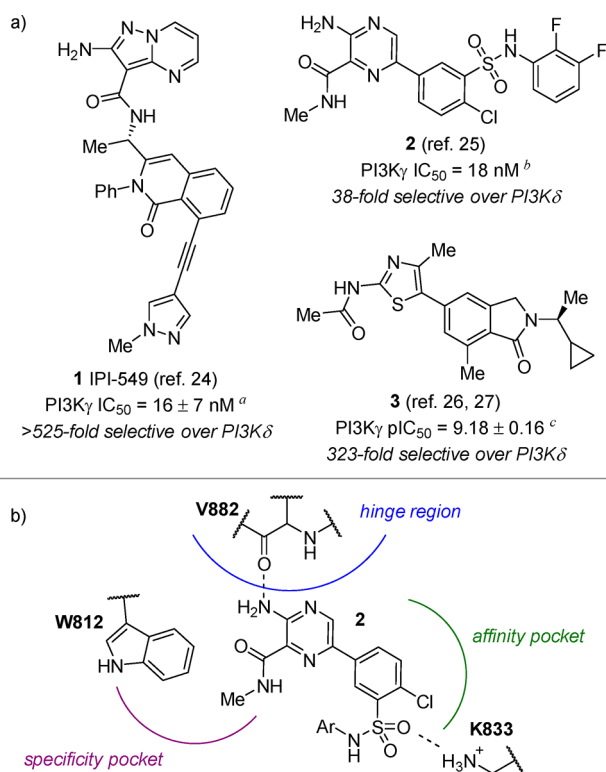
As shown in Figure 1b using aryl sulfonamide **2** as a prototypical example, three regions exist within the ATP binding pocket of PI3K $\gamma$ , which are typically considered during

Received: July 11, 2020

Accepted: September 24, 2020

Published: September 24, 2020





**Figure 1.** (a) Biochemical potency and selectivity values of PI3K $\gamma$ -selective inhibitors, as reported in the literature (see Supporting Information for a comparison of literature and in-house assay protocols). Inhibition determined using the ADP-Glo assay (Promega). Reported ATP  $K_m$  = 29 ± 3.7  $\mu$ M.<sup>34</sup> <sup>a</sup>Assay conditions: 3 mM ATP, 500  $\mu$ M dioctanoyl-phosphatidylinositol-4,5-bisphosphate (diC<sub>8</sub>PIP<sub>2</sub>) as substrate, and 40 nM PI3K $\gamma$ . <sup>b</sup>Assay conditions: 1  $\mu$ M ATP, 10  $\mu$ M PIP<sub>2</sub>, and 30 nM PI3K $\gamma$ . <sup>c</sup>Assay conditions: 20  $\mu$ M ATP, 80  $\mu$ M diC<sub>8</sub>PIP<sub>2</sub>, and 1.2 nM PI3K $\gamma$ . (b) Schematic of typical inhibitor binding modes within PI3K $\gamma$ , exemplified by **2**.<sup>25</sup>

inhibitor design.<sup>33</sup> Interaction with the hinge region is considered essential for inhibitor activity; most known inhibitors engage in at least one hydrogen bond to V882. Inhibitor binding interactions within the affinity pocket are known to considerably influence both potency and selectivity against the other PI3K isoforms, as communicated in the discovery of **3**.<sup>26,27</sup> Most inhibitors that bind within the affinity pocket possess a functional group that engages K833 via hydrogen bonding or polar interactions. Finally, inhibitor binding within the specificity pocket also influences both potency and selectivity, as demonstrated in the discovery of **1**.<sup>24</sup> The W812 side chain in this region of the enzyme–inhibitor complex is well-positioned for an edge-to-face interaction with the inhibitor’s planar motif, as confirmed by the recently reported X-ray co-crystal structure of **1** in complex with human PI3K $\gamma$  (PDB ID 6XRL).<sup>35</sup>

Considering the promise of selective PI3K $\gamma$  inhibition for cancer immunotherapy, we pursued the design of novel inhibitor structures, utilizing the extensive body of medicinal chemistry knowledge as a source of inspiration. Our primary objective was to design a molecule possessing (1) similar or greater PI3K $\gamma$  inhibitory potency and isoform selectivity compared to known inhibitors, such as **1**, as measured in both biochemical and cell-based PI3K $\gamma$  inhibition assays, and (2) suitable ADME properties for use in future *in vivo* studies. A molecule fulfilling these criteria would enable the eventual

deconvolution and appreciation of the role of PI3K $\gamma$  inhibition in the context of our broader immunomodulatory work. To realize these goals, we embarked upon the discovery of novel inhibitors, initially through a pharmacophore mapping approach based on visual comparison of known literature inhibitors followed by a systematic SAR investigation of promising lead molecules, some of which have recently been described.<sup>35</sup>

Due to the high isoform selectivity and potency of **3** (IC<sub>50</sub> = 4 ± 1 nM, as determined in our in-house biochemical assays, which measure a compound’s ability to inhibit the kinase activity of PI3K; see Supporting Information for details) and its analogues,<sup>26,27</sup> we designed an initial set of compounds by attempting to mimic the hinge-binding acylaminothiazole moiety with a variety of functionally similar heterocycles (Table 1). Most of the compounds investigated contained both

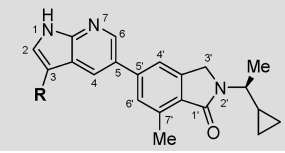
**Table 1.** Modification of the Hinge-Binding Region

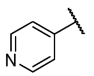
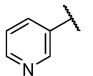
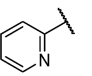
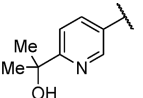
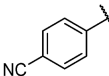
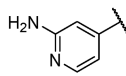
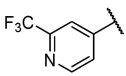
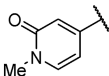
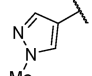
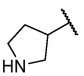
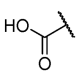
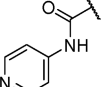
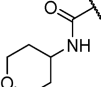
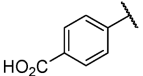
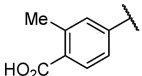
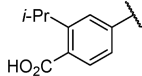
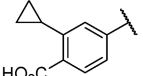
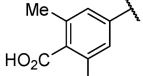
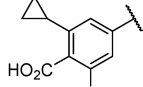
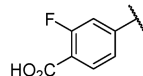
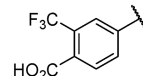
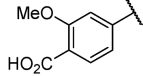
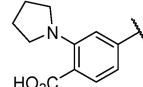
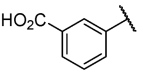
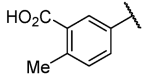
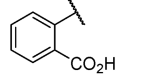
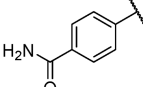
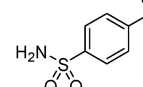
R	PI3K $\gamma$ IC <sub>50</sub> <sup>a</sup>	R	PI3K $\gamma$ IC <sub>50</sub> <sup>a</sup>
	0.6 ± 0.2 $\mu$ M		0.035 ± 0.001 $\mu$ M
	0.53 ± 0.01 $\mu$ M		0.08 ± 0.02 $\mu$ M
	1.6 $\mu$ M <sup>b</sup>		0.05 ± 0.01 $\mu$ M
	0.09 ± 0.01 $\mu$ M		11 8 ± 3 nM
	0.49 ± 0.02 $\mu$ M		12 3.4 ± 0.8 nM
			(R)-12 9 ± 3 nM

<sup>a</sup>IC<sub>50</sub> values measured using the ADP-Glo Lipid Kinase Assay (Promega) with 25  $\mu$ M ATP and 50  $\mu$ M phosphatidylinositol 4,5-bisphosphate as substrate. <sup>b</sup>Compound was tested once.

a hydrogen bond donor and a hydrogen bond acceptor motif, which could potentially create a stronger interaction with V882. We initiated our studies with racemic compounds **4** and **5**, which bear a structural resemblance to **3**. Although potency was substantially reduced for these compounds (IC<sub>50</sub> = 0.6 and 0.53  $\mu$ M, respectively), we were encouraged by the fact that replacement of the aminothiazole motif of **3** did not eliminate activity. Although triazolopyridine **6** showed decreased potency (IC<sub>50</sub> = 1.6  $\mu$ M), a less acidic analogue, (±)-**7**, was significantly more active (IC<sub>50</sub> = 0.09  $\mu$ M). In contrast, an

Table 2. Evaluation of Azaindole C3 Substituents



R							
Compound	<b>12</b>	<b>13<sup>d</sup></b>	<b>14</b>	<b>15</b>	<b>16</b>	<b>17</b>	<b>18</b>
PI3K $\gamma$ IC <sub>50</sub> <sup>a</sup>	3.4 ± 0.8 nM	7 ± 3 nM	33 ± 3 nM	3.3 ± 0.5 nM	42 ± 7 nM	5.8 ± 0.2 nM	16 ± 1 nM
$\alpha/\delta$ Selectivity <sup>b</sup>	379 / 290	89 / 112	>308 / >308	416 / 183	>242 / >242	214 / 640	>578 / >552
PI3K $\gamma$ cellular IC <sub>50</sub> <sup>c</sup>	0.22 ± 0.02 $\mu$ M	0.4 ± 0.3 $\mu$ M	3.5 $\mu$ M <sup>e</sup>	0.6 ± 0.2 $\mu$ M	3.5 $\mu$ M <sup>e</sup>	0.4 $\mu$ M <sup>e</sup>	4 ± 1 $\mu$ M
R							
Compound	<b>19</b>	<b>20</b>	<b>21</b>	<b>22</b>	<b>23</b>	<b>24</b>	<b>25</b>
PI3K $\gamma$ IC <sub>50</sub> <sup>a</sup>	2.6 ± 0.1 nM	3.26 ± 0.06 nM	281 ± 7 nM	13 ± 3 nM	12 ± 2 nM	4.5 ± 0.7 nM	2.5 ± 0.5 nM
$\alpha/\delta$ Selectivity <sup>b</sup>	466 / 128	898 / 379	>36 / >36	>775 / >775	>856 / >856	>2239 / 1033	259 / 136
PI3K $\gamma$ cellular IC <sub>50</sub> <sup>c</sup>	0.20 ± 0.02 $\mu$ M	0.2 ± 0.1 $\mu$ M	3.8 $\mu$ M <sup>e</sup>	11 ± 2 $\mu$ M	1.3 $\mu$ M <sup>e</sup>	0.32 ± 0.02 $\mu$ M	0.14 ± 0.01 $\mu$ M
R							
Compound	<b>26</b>	<b>27</b>	<b>28</b>	<b>29</b>	<b>30</b>	<b>31</b>	<b>32</b>
PI3K $\gamma$ IC <sub>50</sub> <sup>a</sup>	2.8 ± 0.4 nM	2.1 ± 0.2 nM	1.6 ± 0.3 nM	2.2 ± 0.9 nM	1.2 nM <sup>e</sup>	3.1 ± 0.9 nM	1.64 ± 0.05 nM
$\alpha/\delta$ Selectivity <sup>b</sup>	433 / 505	224 / 344	585 / 494	1518 / 1212	691 / 367	546 / 1052	380 / 591
PI3K $\gamma$ cellular IC <sub>50</sub> <sup>c</sup>	0.078 ± 0.006 $\mu$ M	0.059 ± 0.009 $\mu$ M	0.040 ± 0.006 $\mu$ M	0.09 ± 0.03 $\mu$ M	0.07 ± 0.02 $\mu$ M	0.7 ± 0.1 $\mu$ M	0.35 ± 0.08 $\mu$ M
R							
Compound	<b>33</b>	<b>34</b>	<b>35</b>	<b>36</b>	<b>37</b>	<b>38</b>	<b>39</b>
PI3K $\gamma$ IC <sub>50</sub> <sup>a</sup>	1.5 ± 0.1 nM	4 ± 1 nM	2.7 ± 0.9 nM	5 ± 2 nM	180 ± 70 nM	2.59 ± 0.01 nM	5 ± 2 nM
$\alpha/\delta$ Selectivity <sup>b</sup>	369 / 494	853 / 49	321 / 772	>1562 / >1895	>59 / >59	711 / 226	1055 / 463
PI3K $\gamma$ cellular IC <sub>50</sub> <sup>c</sup>	0.17 ± 0.02 $\mu$ M	0.17 ± 0.09 $\mu$ M	0.11 ± 0.04 $\mu$ M	0.26 ± 0.04 $\mu$ M	15 ± 8 $\mu$ M	0.23 ± 0.01 $\mu$ M	0.40 ± 0.06 $\mu$ M

<sup>a</sup>Enzymatic kinase activity assay. <sup>b</sup>Ratio of PI3K $\alpha$  or PI3K $\delta$  enzymatic inhibition over PI3K $\gamma$  inhibition. <sup>c</sup>Determined using the AlphaLISA SureFire Ultra Akt assay (PerkinElmer) with THP-1 cells. <sup>d</sup>Racemate. <sup>e</sup>Compound was tested once.

isomeric analogue, **8**, in which the pyrazole NH group is not properly positioned for interaction with V882, was significantly less potent (IC<sub>50</sub> = 0.49  $\mu$ M), confirming the importance of a hydrogen bond donor and acceptor pair for interaction with the hinge region. The stereochemical configuration of these compounds was also shown to be important, as **7**, the (*S*) enantiomer of ( $\pm$ )-**7**, showed improved activity (IC<sub>50</sub> = 0.035  $\mu$ M) compared to the racemic compound. Although enantiopure pyrazolopyrazine **9** showed a 2-fold reduction in potency (IC<sub>50</sub> = 0.08  $\mu$ M) relative to **7**, azaindole **10** (IC<sub>50</sub> = 0.05  $\mu$ M) had similar inhibitory activity to **7**.

Based on these results and earlier studies by the Meng and Zhou laboratories,<sup>36</sup> we evaluated the incorporation of a 4-pyridyl moiety at the C3 position of the two most promising scaffolds (i.e., azaindazole **7** and azaindole **10**), which we envisioned would provide favorable interactions with the specificity pocket of PI3K $\gamma$ . Consistent with our hypothesis,

azaindazole **11** (IC<sub>50</sub> = 8 nM) was 4-fold more potent than **7**, while azaindole **12** (IC<sub>50</sub> = 3.4 nM) showed an even greater improvement in potency (approximately 15-fold) relative to the unsubstituted analogue, **10**. (*R*)-**12** was 3-fold less potent than **12**, consistent with the previously reported superiority of the (*S*) enantiomer of the isoindolinone moiety of **3**.<sup>26,27</sup> These initial studies established **12** as a suitable starting point for further optimization.

Our subsequent efforts centered on evaluation of various C3-substituted derivatives of **12** (Table 2). To better distinguish between compounds that generally displayed low-nanomolar potency in the biochemical kinase activity assay, we further characterized these inhibitors under more physiologically relevant conditions using a functional cellular inhibition assay, which measures the extent of PI3K-mediated phosphorylation of Akt. To assess PI3K isoform selectivity, we employed routine enzymatic kinase activity assays for the  $\alpha$  and  $\delta$  PI3K

Table 3. Modification of the N2' Substituent

Compound	40	41	42	43	44	45	46	47
PI3K $\gamma$ IC <sub>50</sub> <sup>a</sup>	6 ± 3 nM	6.8 ± 0.2 nM	9 ± 2 nM	50 ± 20 nM	26 nM <sup>d</sup>	28 nM <sup>d</sup>	40 ± 10 nM	25.3 ± 0.2 nM
$\alpha/\delta$ Selectivity <sup>b</sup>	255 / >414	253 / 901	51 / 216	7 / 18	62 / 107	74 / 100	142 / >190	42 / 62
PI3K $\gamma$ cellular IC <sub>50</sub> <sup>c</sup>	0.8 ± 0.5 $\mu$ M	0.8 ± 0.1 $\mu$ M	0.6 ± 0.2 $\mu$ M	1.0 $\mu$ M <sup>d</sup>	0.72 ± 0.04 $\mu$ M	1.1 ± 0.2 $\mu$ M	2.1 $\mu$ M <sup>d</sup>	1.6 $\mu$ M <sup>d</sup>

<sup>a</sup>Enzymatic kinase activity assay. <sup>b</sup>Ratio of PI3K $\alpha$  or PI3K $\delta$  enzymatic inhibition over PI3K $\gamma$  inhibition. <sup>c</sup>Cellular potency in THP-1 cell line. <sup>d</sup>Compound was tested once.

isoforms only, as most of the compounds in this series were inactive against the  $\beta$  isoform at concentrations up to 10  $\mu$ M (>1000-fold selectivity). We were pleased to find that compound **12** exhibited submicromolar activity in THP-1 cells (THP-1 IC<sub>50</sub> = 0.22  $\mu$ M), with excellent isoform selectivity (379-fold vs PI3K $\alpha$  and 290-fold vs PI3K $\delta$ ). The observed difference between biochemical and cellular potency was not surprising, as cellular potency is frequently impacted by a compound's permeability, protein binding, and off-target activity as well as differences in the concentration of ATP present under the assay conditions.

Although the 3-pyridyl analogue **13** (IC<sub>50</sub> = 7 nM, THP-1 IC<sub>50</sub> = 0.4  $\mu$ M) showed comparable potency to **12**, the 2-pyridyl analogue (**14**) was substantially less active (IC<sub>50</sub> = 33 nM, THP-1 IC<sub>50</sub> = 3.5  $\mu$ M), indicating a hydrogen bond acceptor extending outward from the core is advantageous.<sup>37</sup> Other modifications preserving this paradigm (e.g., **15–19**) were either tolerated or had reduced activity, with biochemical potency values ranging from 2.6 to 42 nM, and THP-1 cell potencies ranging from 0.20 to 3.5  $\mu$ M. Pyrazole **20** (IC<sub>50</sub> = 3.26 nM, THP-1 IC<sub>50</sub> = 0.2  $\mu$ M) showed comparable potency to **12**, but incorporation of a saturated, basic amine substituent (e.g., **21**, IC<sub>50</sub> = 281 nM, THP-1 IC<sub>50</sub> = 3.8  $\mu$ M) proved to be detrimental to activity. Interestingly, carboxylic acid **22** and its amide derivatives, **23** and **24**, were moderately active in the biochemical assay (IC<sub>50</sub> = 13, 12, and 4.5 nM, respectively) despite being structurally distinct, although cellular potencies were more variable (THP-1 IC<sub>50</sub> = 11, 1.3, and 0.32  $\mu$ M, respectively).

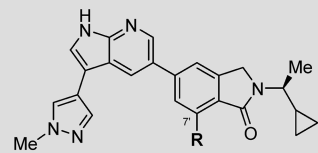
In addition to 5- and 6-membered aromatic heterocycles, benzoic acids were identified as suitable C3 substituents. *para*-Benzoic acid **25** (IC<sub>50</sub> = 2.5 nM, THP-1 IC<sub>50</sub> = 0.14  $\mu$ M), as well as several substituted benzoic acid analogues (**26–30** and **33–35**), exhibited improved cellular potency compared to **20**. The *ortho*-methyl, -isopropyl, and -cyclopropyl analogues of **25** showed an encouraging increase in cellular potency (THP-1 IC<sub>50</sub> = 0.078, 0.059, and 0.040  $\mu$ M, respectively). Disubstituted analogues of **25** (e.g., **29** and **30**, THP-1 IC<sub>50</sub> = 0.09 and 0.07  $\mu$ M, respectively), for which steric effects limit the conformational freedom of the carboxylate group and may attenuate productive interactions within the affinity pocket, showed a minimal reduction in potency relative to the monosubstituted counterparts. Electron-poor benzoic acid derivatives (e.g., **31**

and **32**, THP-1 IC<sub>50</sub> = 0.7 and 0.35  $\mu$ M, respectively) showed a substantial decrease in potency, while analogues bearing electron-donating methoxy or pyrrolidine *ortho*-substituents (e.g., **33** and **34**, THP-1 IC<sub>50</sub> = 0.17  $\mu$ M for both) showed similar potency to unsubstituted benzoic acid **25**.

Interestingly, while *meta*-benzoic acid **35** (THP-1 IC<sub>50</sub> = 0.11  $\mu$ M) exhibited similar potency to the *para*-analogue (**25**), introduction of an *ortho*-methyl substituent to **35** resulted in a 2-fold reduction in potency (**36**, THP-1 IC<sub>50</sub> = 0.26  $\mu$ M). This observation further corroborates the potential effect of the conformation of the carboxylate group on compound potency. In contrast to **25** and **35**, *ortho*-benzoic acid derivative **37** exhibited a dramatic reduction in potency (THP-1 IC<sub>50</sub> = 15  $\mu$ M), consistent with the trends observed for isomeric pyridine analogues **12–14**. Amide and sulfonamide analogues of **25** generally exhibited reduced potency (**38** and **39**, THP-1 IC<sub>50</sub> = 0.23 and 0.40  $\mu$ M, respectively). For the compounds shown in Table 2, cellular potencies generally correlated with biochemical potency. Apart from compounds with a particularly unique geometry (**21**, **22**, and **37**), a modest correlation was observed between cellular potency and biochemical assay-derived lipophilic efficiency values (see Supporting Information for details). Although there was substantial variation of isoform selectivity among the assayed compounds, most of the active compounds exhibited >100-fold selectivity against both PI3K $\alpha$  and  $\delta$ . The highest isoform selectivity was observed for amide **24** and benzoic acid analogues **29** and **36**.

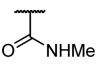

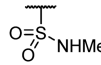
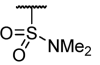

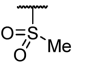
During the course of these investigations into the SAR of the C3 substituent, we also concurrently investigated the SAR of the N2' isoindolinone substituent of **12** (selected due to its combination of potency, selectivity, and structural simplicity), which we envisioned would be situated within the affinity pocket of the PI3K $\gamma$ -inhibitor complex (Table 3). Replacement of the methyl group of the cyclopropylethyl moiety with either an ethyl group (**40**, IC<sub>50</sub> = 6 nM, THP-1 IC<sub>50</sub> = 0.8  $\mu$ M) or a cyclopropyl group (**41**, IC<sub>50</sub> = 6.8 nM, THP-1 IC<sub>50</sub> = 0.8  $\mu$ M) resulted in similar biochemical potency and selectivity but approximately 4-fold reduction in cellular potency. On the other hand, replacement of the cyclopropyl group with a methoxymethylene group (see **42**, IC<sub>50</sub> = 9 nM, THP-1 IC<sub>50</sub> = 0.6  $\mu$ M) resulted in a 3-fold reduction in both biochemical and cellular potency and a substantial reduction in isoform selectivity, confirming the important contribution of the

Table 4. Modification of the C7' Substituent of 20



R	Me	<i>i</i> -Pr	OMe	Cl	CN	CF <sub>3</sub>
Compound	22	48	49	50	51	52
PI3K $\gamma$ IC <sub>50</sub> <sup>a</sup>	3.26 ± 0.06 nM	4.2 ± 0.8 nM	4.3 ± 0.6 nM	2.4 ± 0.2 nM	3.7 ± 0.2 nM	2.4 ± 0.9 nM
$\alpha/\delta$ Selectivity <sup>b</sup>	898 / 379	>1666 / 1378	455 / 365	1059 / 533	2795 / 244	1049 / 266
PI3K $\gamma$ cellular IC <sub>50</sub> <sup>c</sup>	0.2 ± 0.1 $\mu$ M	0.3 ± 0.1 $\mu$ M	0.17 ± 0.07 $\mu$ M	0.17 ± 0.09 $\mu$ M	0.17 ± 0.05 $\mu$ M	0.09 ± 0.02 $\mu$ M

R						
Compound	53	54	55	56	57	58
PI3K $\gamma$ IC <sub>50</sub> <sup>a</sup>	7.9 ± 0.5 nM	2.5 ± 0.9 nM	4 ± 1 nM	2.6 ± 0.9 nM	4 ± 3 nM	1.5 ± 0.3 nM
$\alpha/\delta$ Selectivity <sup>b</sup>	>1060 / >1183	>4159 / >2743	254 / 101	449 / 159	1022 / 615	642 / 289
PI3K $\gamma$ cellular IC <sub>50</sub> <sup>c</sup>	0.73 ± 0.08 $\mu$ M	0.5 ± 0.3 $\mu$ M	0.07 ± 0.01 $\mu$ M	0.10 ± 0.01 $\mu$ M	0.15 ± 0.01 $\mu$ M	0.05 ± 0.02 $\mu$ M

<sup>a</sup>Enzymatic kinase activity assay. <sup>b</sup>Ratio of PI3K $\alpha$  or PI3K $\delta$  enzymatic inhibition over PI3K $\gamma$  inhibition. <sup>c</sup>Cellular potency in THP-1 cell line.

cyclopropyl group to isoform selectivity. An even greater reduction in potency and selectivity was observed for tetrahydropyran **43** (IC<sub>50</sub> = 50 nM, THP-1 IC<sub>50</sub> = 1.0  $\mu$ M), which reinforces the importance of the specific size and shape of the *N*-alkyl substituent. Analogues bearing a sterically bulky *N*-alkyl substituent, such as a *t*-butyl group (**44**, IC<sub>50</sub> = 26 nM, THP-1 IC<sub>50</sub> = 0.72  $\mu$ M), showed diminished potency and isoform selectivity. Similarly, reduced potency and selectivity were observed for analogue **45** (IC<sub>50</sub> = 28 nM), which bears an additional methyl group relative to **12** and is achiral. Despite its large size, arylethane **46** retained modest activity in the biochemical assay (IC<sub>50</sub> = 40 nM), but its potency in cells was significantly decreased (THP-1 IC<sub>50</sub> = 2.1  $\mu$ M) relative to **12**. Compound **47** (THP-1 IC<sub>50</sub> = 1.6  $\mu$ M), which bears an unbranched trifluoroethyl group, exhibited a significant reduction in both potency and selectivity compared to **12**. Taken together, these results indicated that proper substitution of the isoindolinone nitrogen is critical to achieving high potency and selectivity. Moreover, these studies further supported the importance of the cyclopropylethyl group to achieving the optimal balance of potency and isoform selectivity exemplified by **12**.

Further characterization of **12** revealed that it was a potent inhibitor of the major CYP isoforms (IC<sub>50</sub> values for the 1A2, 2D6, 2C9, 2C19, and 3A4 CYP isoforms were 0.7, 2.0, 0.3, <0.1, and 0.3  $\mu$ M, respectively), possibly due to pyridine–iron coordination. On the other hand, pyrazole **20**, which lacks the pyridine moiety, showed an improved CYP inhibition profile (IC<sub>50</sub> values for the 1A2, 2D6, 2C9, 2C19, and 3A4 CYP isoforms were 2.9, 26, 1.4, 0.2, and 0.8  $\mu$ M, respectively). Based on its decreased CYP inhibition and comparable cellular potency to **12**, **20** was selected for further exploration of the isoindolinone substituent.

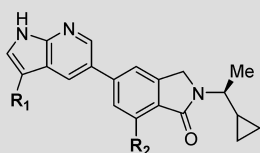
As shown in Table 4, improvement of cellular potency could be realized while maintaining isoform selectivity through various steric and electronic modifications of the C7' group of **20**. Incorporation of a sterically bulky isopropyl group (**48**, THP-1 IC<sub>50</sub> = 0.3  $\mu$ M) had little impact on potency or

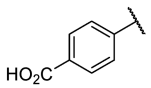
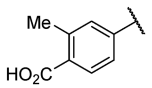
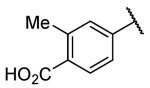
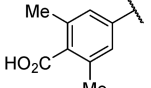
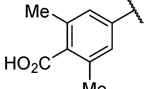
selectivity. Similarly, incorporation of an electron-donating methoxy group (**49**, THP-1 IC<sub>50</sub> = 0.17  $\mu$ M) or electron-withdrawing chloro- or nitrile groups (e.g., **50** and **51**, THP-1 IC<sub>50</sub> = 0.17  $\mu$ M for both) also had little effect on potency or selectivity. Importantly, trifluoromethyl analogue **52** (THP-1 IC<sub>50</sub> = 0.09  $\mu$ M) exhibited a 2-fold improvement in potency over **20** while maintaining high isoform selectivity. While both acetamide isomers **53** and **54** had reduced activity (THP-1 IC<sub>50</sub> = 0.73 and 0.5  $\mu$ M, respectively) relative to **20**, C7'-sulfonamide and -sulfone analogues exhibited up to a 4-fold improvement in potency (**55–58**, THP-1 IC<sub>50</sub> = 0.05–0.15  $\mu$ M). Despite the promising potency of **55** and **58**, these compounds exhibited extrahepatic clearance in rat models (6.0 and 4.5 L/h/kg, respectively), which precluded their further progression.

Faced with the CYP inhibition liabilities of C3-pyridine analogues and the poor metabolic stability of the C3-pyrazole series, we turned our attention to the C3-benzoic acid series, exemplified by analogues **25**, **26**, and **29** (Table 5). Benzoic acid **25** and the corresponding *ortho*-substituted analogue, **26**, both exhibited poor *in vitro* metabolic stability, as measured in human and rat hepatocytes, with rat intrinsic clearance (CL<sub>int</sub>) values  $\geq 40$   $\mu$ L/min/10<sup>6</sup> cells. While hepatocyte stability could be improved through the incorporation of an additional *ortho* substituent on the benzoic acid moiety (**29**, rat CL<sub>int</sub> 2.0  $\mu$ L/min/10<sup>6</sup> cells), this compound exhibited extrahepatic clearance in rat models (e.g., CL = 6.9 L/h/kg). While the C7'-CF<sub>3</sub> analogues of **26** and **29** (see **59** and **60**, THP-1 IC<sub>50</sub> = 0.04 and 0.03  $\mu$ M, respectively) demonstrated improved potency—consistent with our previous observations in the C3-pyrazole series—their metabolic stability was comparable to the C7'-Me analogues. The poor *in vitro/in vivo* correlation for this series of compounds may be due to active efflux, as Caco-2 permeability studies revealed parent compound **25** to have low permeability ( $P_{app}$  = 1.07 × 10<sup>-6</sup> cm/sec) and an efflux ratio of 46.6.

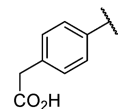
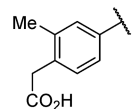
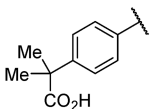
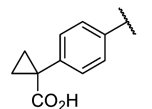
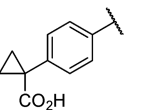
Finally, a breakthrough came with the synthesis of C3 phenylacetic acid derivatives **61** (THP-1 IC<sub>50</sub> = 0.16  $\mu$ M) and

Table 5. Further Characterization and SAR of C3 Benzoic Acid and Phenylacetic Acid Azaindole Derivatives



R <sub>1</sub>					
Compound	25 (R <sub>2</sub> = Me)	26 (R <sub>2</sub> = Me)	59 (R <sub>2</sub> = CF <sub>3</sub> )	29 (R <sub>2</sub> = Me)	60 (R <sub>2</sub> = CF <sub>3</sub> )
PI3K $\gamma$ IC <sub>50</sub> <sup>a</sup>	2.5 ± 0.5 nM	2.8 ± 0.4 nM	1.2 ± 0.1 nM	2.2 ± 0.9 nM	2.8 nM <sup>d</sup>
$\alpha/\delta$ Selectivity <sup>b</sup>	259 / 136	433 / 505	918 / 335	1518 / 1212	257 / 84
PI3K $\gamma$ cellular IC <sub>50</sub> <sup>c</sup>	0.14 ± 0.01 $\mu$ M	0.08 ± 0.01 $\mu$ M	0.04 ± 0.01 $\mu$ M	0.09 ± 0.03 $\mu$ M	0.03 ± 0.01 $\mu$ M
Hepatocyte CL <sub>int</sub> ( $\mu$ L/min/10 <sup>6</sup> cells)	human: 24 rat: 54	human: 19 rat: 51	human: 20 rat: 46	human: <1.2 rat: 2.0	human: 1.8 rat: <1.2
<i>in vivo</i> CL (rat) <sup>e</sup>	11 L/h/kg	n.d.	n.d.	6.9 L/h/kg	28 L/h/kg

R <sub>1</sub>					
Compound	61 (R <sub>2</sub> = Me)	62 (R <sub>2</sub> = Me)	63 (R <sub>2</sub> = Me)	64 (R <sub>2</sub> = Me)	65 (R <sub>2</sub> = CF <sub>3</sub> )
PI3K $\gamma$ IC <sub>50</sub> <sup>a</sup>	2.6 ± 0.2 nM	3.3 nM <sup>d</sup>	2.1 nM <sup>d</sup>	3.3 ± 0.4 nM	3.6 ± 0.6 nM
$\alpha/\delta$ Selectivity <sup>b</sup>	878 / 872	539 / 397	835 / 968	863 / 1401	742 / 620
PI3K $\gamma$ cellular IC <sub>50</sub> <sup>c</sup>	0.16 ± 0.02 $\mu$ M	0.15 ± 0.07 $\mu$ M	0.18 ± 0.02 $\mu$ M	0.15 ± 0.04 $\mu$ M	0.11 ± 0.02 $\mu$ M
Hepatocyte CL <sub>int</sub> ( $\mu$ L/min/10 <sup>6</sup> cells)	human: 6.9 rat: 17	human: 8.0 rat: 23	human: 2.3 rat: 27	human: 1.7 rat: 16	human: 2.6 rat: 18
<i>in vivo</i> CL (rat) <sup>e</sup>	n.d.	1.8 L/h/kg	n.d.	1.8 L/h/kg	n.d.

<sup>a</sup>Enzymatic kinase activity assay. <sup>b</sup>Ratio of PI3K $\alpha$  or PI3K $\delta$  enzymatic inhibition over PI3K $\gamma$  inhibition. <sup>c</sup>Cellular potency in THP-1 cell line. <sup>d</sup>Compound was tested once. <sup>e</sup>n.d. = value not determined.

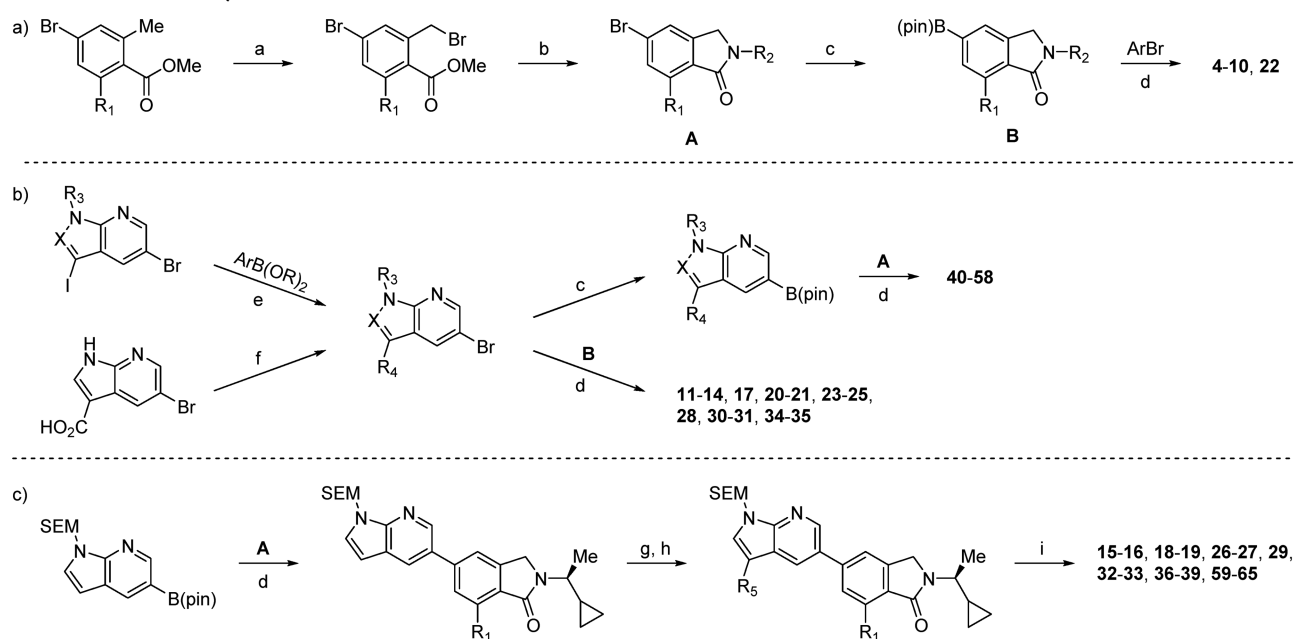
62 (THP-1 IC<sub>50</sub> = 0.15  $\mu$ M). Although these molecules showed somewhat diminished inhibitory activity relative to the benzoic acids, they retained high isoform selectivity and displayed an encouraging improvement in hepatocyte stability (rat CL<sub>int</sub> = 17 and 23  $\mu$ L/min/10<sup>6</sup> cells for 61 and 62, respectively). Moreover, compound 62 exhibited significantly lower *in vivo* clearance (CL = 1.8 L/h/kg) relative to the benzoic acid analogues, which lack a methylene spacer. Gratifyingly, substitution of the  $\alpha$ -methylene group of 61 (see 63–65, THP-1 IC<sub>50</sub> = 0.11–0.18  $\mu$ M) resulted in further improvements in human hepatocyte stability without substantially altering the potency or selectivity of these inhibitors. While this optimization campaign did not ultimately deliver a compound suitable for further development, compound 64 emerged as the most promising inhibitor due to its high cellular potency, excellent isoform selectivity, and acceptable pharmacokinetic profile.

The general synthetic routes used to access our azaindole/azaindazole inhibitors are shown in Scheme 1. The overall sequence is highly modular and allows for the introduction of diversity in several independent steps. Depending on the specific substrate, conditions such as the coupling partner, palladium catalyst, base, or solvent may vary (see Supporting

Information for details). In general, the respective coupling steps can be done in any order to facilitate SAR exploration.

As shown in Scheme 1a, isoindolinone intermediates A and B are generated from methyl benzoate and primary amine precursors. These can be coupled to a variety of heteroaryl bromides to yield various simple inhibitors (4–10, 22). Alternatively, A or B can be coupled with C3-substituted azaindole/azaindazole intermediates, as shown in Scheme 1b. This sequence proved particularly useful during SAR evaluation of isoindolinone substituents. Finally, the sequence shown in Scheme 1c enabled rapid evaluation of C3 aryl substituents in combination with the most promising isoindolinone scaffolds.

Traditionally, ligand interactions within the affinity and specificity pockets of PI3K $\gamma$  have been thought to independently affect potency and selectivity, respectively. In contrast, our SAR investigations demonstrate that improvements in both metrics can be realized through careful design of inhibitors that are capable of occupying both regions of the enzyme active site. Through systematic SAR analysis, we have discovered a series of novel, potent, and selective azaindole-based PI3K $\gamma$  inhibitors. These compounds exhibit cellular IC<sub>50</sub> values as low as 0.040  $\mu$ M (28), while maintaining >300-fold selectivity against all other class I PI3K isoforms. In further

Scheme 1. General Synthetic Routes to Azaindole-Based Inhibitors<sup>a</sup>

<sup>a</sup>Reagents and conditions: (a) NBS, (PhCO<sub>2</sub>)<sub>2</sub>, CCl<sub>4</sub>, 80 °C; (b) RNH<sub>2</sub>, B(OH)<sub>3</sub>, K<sub>2</sub>CO<sub>3</sub>, ACN, r.t.; (c) B<sub>2</sub>pin<sub>2</sub>, (dppf)PdCl<sub>2</sub>, KOAc, dioxane, 100 °C; (d) (dppf)PdCl<sub>2</sub>, Na<sub>2</sub>CO<sub>3</sub>, dioxane/H<sub>2</sub>O, 100 °C; then deprotection (conditions vary, see Supporting Information); (e) (dppf)PdCl<sub>2</sub>, Na<sub>2</sub>CO<sub>3</sub>, dioxane/H<sub>2</sub>O, 80 °C; (f) RNH<sub>2</sub>, HATU, *i*-Pr<sub>2</sub>NEt, DMF, 40 °C; (g) NBS, CH<sub>2</sub>Cl<sub>2</sub>, r.t.; (h) ArB(OR)<sub>2</sub>, (dppf)PdCl<sub>2</sub>, Na<sub>2</sub>CO<sub>3</sub>, dioxane/H<sub>2</sub>O, 100 °C; (i) TFA, r.t.; *N,N*-DMEDA, MeOH, 45 °C.

inhibitor design iterations, C3 phenylacetic acid derivatives (e.g., **64**) exhibited significantly improved pharmacokinetic properties, helping pave the way for future biological studies. The volume of data generated in this study will help expedite future campaigns toward potent and orally bioavailable PI3K $\gamma$  inhibitors for potential clinical applications.

## ■ ASSOCIATED CONTENT

### Supporting Information

The Supporting Information is available free of charge at <https://pubs.acs.org/doi/10.1021/acsmchemlett.0c00387>.

Biological assay procedures, synthetic procedures and characterization of PI3K $\gamma$  inhibitors (PDF)

## ■ AUTHOR INFORMATION

### Corresponding Author

Jenna L. Jeffrey – Arcus Biosciences, Inc., Hayward, California 94545, United States; [orcid.org/0000-0001-9249-5984](https://orcid.org/0000-0001-9249-5984); Email: [jjeffrey@arcusbio.com](mailto:jjeffrey@arcusbio.com)

### Authors

Dillon H. Miles – Arcus Biosciences, Inc., Hayward, California 94545, United States  
 Xuelei Yan – Arcus Biosciences, Inc., Hayward, California 94545, United States  
 Rhiannon Thomas-Tran – Arcus Biosciences, Inc., Hayward, California 94545, United States  
 Jeremy Fournier – Arcus Biosciences, Inc., Hayward, California 94545, United States  
 Ehesan U. Sharif – Arcus Biosciences, Inc., Hayward, California 94545, United States; [orcid.org/0000-0002-2605-6745](https://orcid.org/0000-0002-2605-6745)  
 Samuel L. Drew – Arcus Biosciences, Inc., Hayward, California 94545, United States

Guillaume Mata – Arcus Biosciences, Inc., Hayward, California 94545, United States; [orcid.org/0000-0001-8064-8699](https://orcid.org/0000-0001-8064-8699)

Kenneth V. Lawson – Arcus Biosciences, Inc., Hayward, California 94545, United States; [orcid.org/0000-0001-5094-6337](https://orcid.org/0000-0001-5094-6337)

Elaine Ginn – Arcus Biosciences, Inc., Hayward, California 94545, United States

Kent Wong – Arcus Biosciences, Inc., Hayward, California 94545, United States

Divyank Soni – Arcus Biosciences, Inc., Hayward, California 94545, United States

Puja Dhanota – Arcus Biosciences, Inc., Hayward, California 94545, United States

Stefan G. Shaqfeh – Arcus Biosciences, Inc., Hayward, California 94545, United States

Cesar Meleza – Arcus Biosciences, Inc., Hayward, California 94545, United States

Ada Chen – Arcus Biosciences, Inc., Hayward, California 94545, United States

Amber T. Pham – Arcus Biosciences, Inc., Hayward, California 94545, United States

Timothy Park – Arcus Biosciences, Inc., Hayward, California 94545, United States

Debbie Swinarski – Arcus Biosciences, Inc., Hayward, California 94545, United States

Jesus Banuelos – Arcus Biosciences, Inc., Hayward, California 94545, United States

Ulrike Schindler – Arcus Biosciences, Inc., Hayward, California 94545, United States

Matthew J. Walters – Arcus Biosciences, Inc., Hayward, California 94545, United States

Nigel P. Walker – Arcus Biosciences, Inc., Hayward, California 94545, United States

Xiaoning Zhao – Arcus Biosciences, Inc., Hayward, California 94545, United States

Stephen W. Young – Arcus Biosciences, Inc., Hayward, California 94545, United States

Jie Chen – Arcus Biosciences, Inc., Hayward, California 94545, United States; [orcid.org/0000-0002-3093-6665](https://orcid.org/0000-0002-3093-6665)

Lixia Jin – Arcus Biosciences, Inc., Hayward, California 94545, United States

Manmohan Reddy Leleti – Arcus Biosciences, Inc., Hayward, California 94545, United States

Jay P. Powers – Arcus Biosciences, Inc., Hayward, California 94545, United States

Complete contact information is available at:  
<https://pubs.acs.org/10.1021/acsmchemlett.0c00387>

### Author Contributions

D.H.M. and J.L.J. wrote the manuscript; D.H.M., J.L.J., E.U.S., G.M., K.V.L., M.R.L., and J.P.P. edited the manuscript; J.L.J., X.Y., R.T.-T., J.F., E.U.S., D.H.M., G.M., S.D., K.V.L., M.R.L., and J.P.P. contributed to inhibitor design; J.L.J., X.Y., R.T.-T., J.F., E.U.S., D.H.M., G.M., S.D., and K.V.L. synthesized the inhibitors; E.G., K.W., D.S., P.D., T.P., D.S., J.C., and L.J. provided ADME support; S.G.S., C.M., A.C., X.Z., S.W.Y. provided biological assay support; A.P., U.S., and N.P.W. provided protein support. All authors have given approval to the final version of the manuscript.

### Notes

The authors declare the following competing financial interest(s): All authors are current or former employees of Arcus Biosciences.

### ABBREVIATIONS

SAR, structure–activity relationship; ATP, adenosine triphosphate; ADME, absorption, distribution, metabolism, and excretion; CYP, cytochrome P450; NBS, *N*-bromosuccinimide; ACN, acetonitrile; r.t., room temperature (23 °C); pin, pinacolato; dppf, 1,1'-bis(diphenylphosphino)ferrocene; HATU, (1-[bis(dimethylamino)methylene]-1*H*-1,2,3-triazolo[4,5-*b*]pyridinium 3-oxide hexafluorophosphate); DMF, *N,N*-dimethylformamide; SEM, 2-(trimethylsilyl)ethoxymethyl; TFA, trifluoroacetic acid; *N,N*-DMEDA, *N,N*-dimethylethane-1,2-diamine

### REFERENCES

- (1) Wymann, M. P.; Pirola, L. Structure and Function of Phosphoinositide 3-Kinases. *Biochim. Biophys. Acta, Mol. Cell Biol. Lipids* **1998**, *1436*, 127–150.
- (2) Amzel, L. M.; Huang, C.-H.; Mandelker, D.; Lengauer, C.; Gabelli, S. B.; Vogelstein, B. Structural Comparisons of Class I Phosphoinositide 3-Kinases. *Nat. Rev. Cancer* **2008**, *8*, 665–669.
- (3) Toker, A.; Cantley, L. C. Signalling through the Lipid Products of Phosphoinositide-3-OH Kinase. *Nature* **1997**, *387*, 673–676.
- (4) Cahill, C. M.; Rogers, J. T.; Walker, W. A. The Role of Phosphoinositide 3-Kinase Signaling in Intestinal Inflammation. *J. Signal Transduction* **2012**, *2012*, 1–13.
- (5) Sasaki, T.; Irie-Sasaki, J.; Jones, R. G.; Oliveira-Dos-Santos, A. J.; Stanford, W. L.; Bolon, B.; Wakeham, A.; Itie, A.; Bouchard, D.; Kozieradzki, I.; Joza, N.; Mak, T. W.; Ohashi, P. S.; Suzuki, A.; Penninger, J. M. Function of PI3K $\gamma$  in Thymocyte Development, T Cell Activation, and Neutrophil Migration. *Science* **2000**, *287*, 1040–1046.
- (6) Kaneda, M. M.; Messer, K. S.; Ralainirina, N.; Li, H.; Leem, C. J.; Gorjestani, S.; Woo, G.; Nguyen, A. V.; Figueiredo, C. C.; Foubert, P.; Schmid, M. C.; Pink, M.; Winkler, D. G.; Rausch, M.; Palombella, V. J.; Kutok, J.; McGovern, K.; Frazer, K. A.; Wu, X.; Karin, M.; Sasik,

R.; Cohen, E. E. W.; Varner, J. A. PI3K $\gamma$  Is a Molecular Switch That Controls Immune Suppression. *Nature* **2016**, *539*, 437–442.

(7) González-García, A.; Sánchez-Ruiz, J.; Flores, J. M.; Carrera, A. C. Phosphatidylinositol 3-Kinase  $\gamma$  Inhibition Ameliorates Inflammation and Tumor Growth in a Model of Colitis-Associated Cancer. *Gastroenterology* **2010**, *138*, 1374–1383.

(8) Fruman, D. A.; Rommel, C. PI3K and Cancer: Lessons, Challenges and Opportunities. *Nat. Rev. Drug Discovery* **2014**, *13*, 140–156.

(9) Stark, A. K.; Sriskantharajah, S.; Hessel, E. M.; Okkenhaug, K. PI3K Inhibitors in Inflammation, Autoimmunity and Cancer. *Curr. Opin. Pharmacol.* **2015**, *23*, 82–91.

(10) Thorpe, L. M.; Yuzugullu, H.; Zhao, J. J. PI3K in Cancer: Divergent Roles of Isoforms, Modes of Activation and Therapeutic Targeting. *Nat. Rev. Cancer* **2015**, *15*, 7–24.

(11) Kaneda, M. M.; Cappello, P.; Nguyen, A. V.; Ralainirina, N.; Hardamon, C. R.; Foubert, P.; Schmid, M. C.; Sun, P.; Mose, E.; Bouvet, M.; Lowy, A. M.; Valasek, M. A.; Sasik, R.; Novelli, F.; Hirsch, E.; Varner, J. A. Macrophage PI3K $\gamma$  Drives Pancreatic Ductal Adenocarcinoma Progression. *Cancer Discovery* **2016**, *6*, 870–885.

(12) Janku, F. Phosphoinositide 3-Kinase (PI3K) Pathway Inhibitors in Solid Tumors: From Laboratory to Patients. *Cancer Treat. Rev.* **2017**, *59*, 93–101.

(13) Zhao, H.-F.; Wang, J.; Shao, W.; Wu, C.-P.; Chen, Z.-P.; To, S.-S. T.; Li, W.-P. Recent Advances in the Use of PI3K Inhibitors for Glioblastoma Multiforme: Current Preclinical and Clinical Development. *Mol. Cancer* **2017**, *16*, 1–16.

(14) Zhao, W.; Qiu, Y.; Kong, D. Class I Phosphatidylinositol 3-Kinase Inhibitors for Cancer Therapy. *Acta Pharm. Sin. B* **2017**, *7*, 27–37.

(15) Joshi, S.; Durden, D. L. Combinatorial Approach to Improve Cancer Immunotherapy: Rational Drug Design Strategy to Simultaneously Hit Multiple Targets to Kill Tumor Cells and to Activate the Immune System. *J. Oncol.* **2019**, *2019*, 1–18.

(16) Fruman, D. A. Targeting PI3K-Gamma in Non-Hodgkin Lymphoma. *J. Clin. Oncol.* **2019**, *37*, 932–934.

(17) De Henau, O.; Rausch, M.; Winkler, D.; Campesato, L. F.; Liu, C.; Cymerman, D. H.; Budhu, S.; Ghosh, A.; Pink, M.; Tchaicha, J.; Douglas, M.; Tibbitts, T.; Sharma, S.; Proctor, J.; Kosmider, N.; White, K.; Stern, H.; Soglia, J.; Adams, J.; Palombella, V. J.; McGovern, K.; Kutok, J. L.; Wolchok, J. D.; Merghoub, T. Overcoming Resistance to Checkpoint Blockade Therapy by Targeting PI3K $\gamma$  in Myeloid Cells. *Nature* **2016**, *539*, 443–447.

(18) Cassetta, L.; Kitamura, T. Targeting Tumor-Associated Macrophages as a Potential Strategy to Enhance the Response to Immune Checkpoint Inhibitors. *Front. Cell Dev. Biol.* **2018**, *6*, 1–6.

(19) Perry, M. W. D.; Abdulai, R.; Mogemark, M.; Petersen, J.; Thomas, M. J.; Valastro, B.; Westin Eriksson, A. Evolution of PI3K $\gamma$  and  $\delta$  Inhibitors for Inflammatory and Autoimmune Diseases. *J. Med. Chem.* **2019**, *62*, 4783–4814.

(20) Garces, A. E.; Stocks, M. J. Class I PI3K Clinical Candidates and Recent Inhibitor Design Strategies: A Medicinal Chemistry Perspective. *J. Med. Chem.* **2019**, *62*, 4815–4850.

(21) Come, J. H.; Collier, P. N.; Henderson, J. A.; Pierce, A. C.; Davies, R. J.; Le Tiran, A.; O'Dowd, H.; Bandarage, U. K.; Cao, J.; Deiningner, D.; Grey, R.; Krueger, E. B.; Lowe, D. B.; Liang, J.; Liao, Y.; Messersmith, D.; Nanthakumar, S.; Sizensky, E.; Wang, J.; Xu, J.; Chin, E. Y.; Damagnez, V.; Doran, J. D.; Dworakowski, W.; Griffith, J. P.; Jacobs, M. D.; Khare-Pandit, S.; Mahajan, S.; Moody, C. S.; Aronov, A. M. Design and Synthesis of a Novel Series of Orally Bioavailable, CNS-Penetrant, Isoform Selective Phosphoinositide 3-Kinase  $\gamma$  (PI3K $\gamma$ ) Inhibitors with Potential for the Treatment of Multiple Sclerosis (MS). *J. Med. Chem.* **2018**, *61*, 5245–5256.

(22) Shvartsbart, A.; Combs, A. P.; Falahatpisheh, N.; Polam, P.; Shao, L.; Shepard, S. 3-(5-Amino-pyrazin-2-yl)-benzenesulfonamide Derivatives and Related Compounds as PI3K-gamma Kinase Inhibitors for Treating Cancer. WIPO 2019, WO 2019/126505 A1.

(23) Bellenie, B. R.; Bloomfield, G. C.; Bruce, I.; Culshaw, A. J.; Hall, E. C.; Hollingworth, G.; Neef, J.; Spendiff, M.; Watson, S. J. Amino



Pyrazine Derivatives as Phosphatidylinositol 3-Kinase Inhibitors. WIPO 2015, WO 2015/162459 A1.

(24) Evans, C. A.; Liu, T.; Lescarbeau, A.; Nair, S. J.; Grenier, L.; Pradeilles, J. A.; Glenadel, Q.; Tibbitts, T.; Rowley, A. M.; Dinitto, J. P.; Brophy, E. E.; O'Hearn, E. L.; Ali, J. A.; Winkler, D. G.; Goldstein, S. I.; O'Hearn, P.; Martin, C. M.; Hoyt, J. G.; Soglia, J. R.; Cheung, C.; Pink, M. M.; Proctor, J. L.; Palombella, V. J.; Tremblay, M. R.; Castro, A. C. Discovery of a Selective Phosphoinositide-3-Kinase (PI3K)- $\gamma$  Inhibitor (IPI-549) as an Immuno-Oncology Clinical Candidate. *ACS Med. Chem. Lett.* **2016**, *7*, 862–867.

(25) Leahy, J. W.; Buhr, C. A.; Johnson, H. W. B.; Kim, B. G.; Baik, T.; Cannoy, J.; Forsyth, T. P.; Jeong, J. W.; Lee, M. S.; Ma, S.; Noson, K.; Wang, L.; Williams, M.; Nuss, J. M.; Brooks, E.; Foster, P.; Goon, L.; Heald, N.; Holst, C.; Jaeger, C.; Lam, S.; Lougheed, J.; Nguyen, L.; Plonowski, A.; Song, J.; Stout, T.; Wu, X.; Yakes, M. F.; Yu, P.; Zhang, W.; Lamb, P.; Raeber, O. Discovery of a Novel Series of Potent and Orally Bioavailable Phosphoinositide 3-Kinase  $\gamma$  Inhibitors. *J. Med. Chem.* **2012**, *55*, 5467–5482.

(26) Pemberton, N.; Mogemark, M.; Arlbrandt, S.; Bold, P.; Cox, R. J.; Gardelli, C.; Holden, N. S.; Karabelas, K.; Karlsson, J.; Lever, S.; Li, X.; Lindmark, H.; Norberg, M.; Perry, M. W. D.; Petersen, J.; Blomqvist, S. R.; Thomas, M.; Tyrchan, C.; Eriksson, A. W.; Zlatoidsky, P.; Öster, L. Discovery of Highly Isoform Selective Orally Bioavailable Phosphoinositide 3-Kinase (PI3K)- $\gamma$  Inhibitors. *J. Med. Chem.* **2018**, *61*, 5435–5441.

(27) Gangadhara, G.; Dahl, G.; Bohnacker, T.; Rae, R.; Gunnarsson, J.; Blaho, S.; Öster, L.; Lindmark, H.; Karabelas, K.; Pemberton, N.; Tyrchan, C.; Mogemark, M.; Wymann, M. P.; Williams, R. L.; Perry, M. W. D.; Papavoine, T.; Petersen, J. A Class of Highly Selective Inhibitors Bind to an Active State of PI3K $\gamma$ . *Nat. Chem. Biol.* **2019**, *15*, 348–357.

(28) A Dose-Escalation Study to Evaluate the Safety, Tolerability, Pharmacokinetics, and Pharmacodynamics of IPI-549. Last updated May 28, 2020. <https://clinicaltrials.gov/ct2/show/NCT02637531> (accessed Jul 10, 2020).

(29) A Study to Evaluate Safety/Tolerability of Immunotherapy Combinations in Participants With Triple-Negative Breast Cancer or Gynecologic Malignancies. Last updated Jul 8, 2020. <https://clinicaltrials.gov/ct2/show/NCT03719326> (accessed Jul 10, 2020).

(30) Window of Opportunity Study of IPI-549 in Patients With Locally Advanced HPV+ and HPV- Head and Neck Squamous Cell Carcinoma. Last updated May 21, 2020. <https://clinicaltrials.gov/ct2/show/NCT03795610> (accessed Jul 10, 2020).

(31) Study to Evaluate the Efficacy/Safety of IPI-549 in Combination With Nivolumab in Patients With Advanced Urothelial Carcinoma (MARIO-275). Last updated May 18, 2020. <https://clinicaltrials.gov/ct2/show/NCT03980041> (accessed Jul 10, 2020).

(32) Evaluation of IPI-549 Combined With Front-line Treatments in Pts. With Triple-Negative Breast Cancer or Renal Cell Carcinoma (MARIO-3). Last updated May 18, 2020. <https://clinicaltrials.gov/ct2/show/NCT03961698> (accessed Jul 10, 2020).

(33) Miller, M. S.; Thompson, P. E.; Gabelli, S. B. Structural Determinants of Isoform Selectivity in PI3K Inhibitors. *Biomolecules* **2019**, *9*, 1–35.

(34) Vidugiriene, J.; Zegzouti, H.; Goueli, S. A. Evaluating the Utility of a Bioluminescent ADP-Detecting Assay for Lipid Kinases. *Assay Drug Dev. Technol.* **2009**, *7*, 585–597.

(35) Drew, S. L.; Thomas-Tran, R.; Beatty, J. W.; Fournier, J.; Lawson, K. V.; Miles, D. H.; Mata, G.; Sharif, E. U.; Yan, X.; Mailyan, A. K.; Ginn, E.; Chen, J.; Wong, K.; Soni, D.; Dhanota, P.; Chen, P.-Y.; Shaqfeh, S. G.; Meleza, C.; Pham, A. T.; Chen, A.; Zhao, X.; Banuelos, J.; Jin, L.; Schindler, U.; Walters, M. J.; Young, S. W.; Walker, N. P.; Leleti, M. R.; Powers, J. P.; Jeffrey, J. L. Discovery of Potent and Selective PI3K $\gamma$  Inhibitors. *J. Med. Chem.* **2020**, Article ASAP, DOI: 10.1021/acsmchem.0c01203.

(36) Yang, C.; Zhang, X.; Wang, Y.; Yang, Y.; Liu, X.; Deng, M.; Jia, Y.; Ling, Y.; Meng, L.-H.; Zhou, Y. Discovery of a Novel Series of 7-Azaindole Scaffold Derivatives as PI3K Inhibitors with Potent Activity. *ACS Med. Chem. Lett.* **2017**, *8*, 875–880.

(37) The 2-pyridyl substituent may also differentially affect the electronics of the central core, potentially decreasing the azaindole binding affinity to the hinge region of the enzyme.